Atmos. Meas. Tech. Discuss., 4, 1989–2005, 2011
www.atmos-meas-tech-discuss.net/4/1989/2011/
doi:10.5194/amtd-4-1989-2011

Atmospheric Measurement Techniques Discussions

Observation of slant column NO_2 using the super-zoom mode of AURA-OMI

L. C. Valin[1], A. R. Russell[1], E. J. Bucsela[2], J. P. Veefkind[3], and R. C. Cohen[1,4]

[1]College of Chemistry, University of California Berkeley, Berkeley, CA 94720, USA
[2]SRI International, Menlo Park, CA 94025, USA
[3]Royal Netherlands Meteorological Institute (KNMI), De Bilt, The Netherlands
[4]Department of Earth and Planetary Sciences, University of California Berkeley, Berkeley, CA 94720, USA

Received: 8 February 2011 – Accepted: 18 March 2011 – Published: 29 March 2011

Correspondence to: R. C. Cohen (rccohen@berkeley.edu)

Published by Copernicus Publications on behalf of the European Geosciences Union.

Abstract

We retrieve slant column NO_2 from the super-zoom mode of the Ozone Monitoring Instrument (OMI) to explore its utility for understanding NO_x emissions and removal. Slant column NO_2 is operationally retrieved from OMI at $13 \times 24\,km^2$, a nadir footprint resulting from the on-board average of eight detector elements. For 85 orbits in late 2004, OMI reported observations from individual "super-zoom" detector elements (spaced at $13 \times 3\,km^2$ at nadir). We assess the spatial response of these individual detector elements in-flight and determine an upper-bound on spatial resolution of 9 km, in good agreement with on-ground calibration (7 km FWHM). We retrieve slant column NO_2 from these super-zoom observations over Sarni, India (19 November), Seoul, South Korea (21 November), Dubai, United Arab Emirates (21 November) and the Rihand Reservoir in India (23 November) using differential optical absorption spectroscopy. Comparison of super-zoom and operational-scale retrievals highlights the capacity of the super-zoom mode to distinguish NO_x sources in close proximity. The 1-σ signal to noise ratio (SNR) for these retrievals is as high as 25 and is greater than 5 over the observed enhancements indicating that instrumental noise is not the limitation to obtaining high spatial resolution NO_2 maps. We show that these high resolution observations provide constraints on NO_2 gradients providing a direct measure of the NO_x lifetime in the near field of large plumes.

1 Introduction

Nitrogen oxides ($NO_x \equiv NO + NO_2$) exhibit strong control over tropospheric ozone production and HO_x ($HO_2 + RO_2 + HO$) cycling. Despite a relatively short chemical lifetime (τ_{NO_x} ~1.5 h–1 day in the planetary boundary layer), NO_x emitted locally can result in perturbations to atmospheric composition that extend for hundreds of kilometers, in part due to atmospheric processing that stores and releases NO_x, but also in part due to the magnitude of the source being many e-folds in excess of the global background.

AMTD
4, 1989–2005, 2011

Satellite-based UV/Visible mapping spectrometers provide a comprehensive view of the global and regional patterns of NO_2 columns (e.g. Jaegle et al., 2005; Richter et al., 2005; Russell et al., 2010). Interpretation of these observations has primarily been via chemical transport models (grid spacing ≈ 100 km) that assume chemical processing is accurately represented (e.g. Martin et al., 2003; Toenges-Schuller et al., 2006; Konovalov et al., 2006; Kim et al., 2006). Many of these models have resolution that is coarse compared to both the e-folding decay length of an NO_2 plume and the spatial resolution provided by the satellite instruments. High resolution observations offer the possibility of direct measurement of the spatial gradients in the NO_2 column in regions where such gradients depend on the chemical loss rates of NO_2 more strongly than on emissions. The resolution needed for such analyses is still a subject of research (e.g. Loughner et al., 2007); however, it seems likely to be in the range of 3–10 km.

Here we use observations from OMI (Levelt et al., 2006a, b) to retrieve slant column NO_2 at high spatial resolution. We test the spatial resolution of the OMI super-zoom mode (Sect. 3), and then retrieve slant column NO_2 over several source types (Sect. 4) briefly describing the DOAS fit error (Sect. 5). We discuss the implications of the enhanced spatial resolution on our understanding of NO_x removal rate in the context of observations of Dubai, UAE (Sect. 6).

2 Methods

OMI sits aboard the sun-synchronous, polar-orbiting NASA Aura satellite (Schoeberl et al., 2006), measuring solar and backscattered UV/Visible radiance with a standard operational footprint of $13 \times 24\,km^2$ at nadir, an average of eight detector elements (Levelt et al., 2006a, b). OMI operated in a non-standard "super-zoom" mode for 85 orbits in 2004 reporting data from each detector element. Due to data transmission constraints, this increase in spatial sampling requires a corresponding decrease in spatial coverage such that a single super-zoom orbit covers only 180 km of the 2600 km operational-mode swath width.

AMTD
4, 1989–2005, 2011

We use the level 1b calibrated, wavelength-corrected OMI radiance (OML1BRVZ, OML1BRVG v.3) and solar irradiance (OML1BRR v.3) data recorded on the Goddard Earth Sciences Data and Information Services Center (GES-DISC, http://disc.sci.gsfc.nasa.gov/Aura/data-holdings/OMI) (Van den Oord et al., 2006; Dobber et al., 2008). Observed earthshine spectra are divided by the average of solar spectra from 2005 to obtain top-of-atmosphere reflectance spectra. It has been shown that the averaging of solar spectra reduces noise and detector anomalies known as "striping" in the NO_2 retrieval (Celarier et al., 2008; Dobber et al., 2006).

Slant column NO_2 is retrieved using a DOAS linear least squares fit (Platt and Stutz, 2008; Wenig et al., 2005) as in the operational DOAS retrievals (Boersma et al., 2007; Bucsela et al., 2006). The observed reflectance spectra are fit to a slowly varying third order polynomial, an NO_2 cross section ($T = 220$ K; Vandaele et al., 2002), an O_3 cross section ($T = 220$ K; Bogumil et al., 2001), and a linear term correcting for the ring effect ($T = 220$ K; Chance and Spurr, 1997) over the 405–465 nm spectral window. Spectra for water and the O_2 dimer are not included in the DOAS fit as previous retrievals found their inclusion unnecessary (Boersma et al., 2007; Bucsela et al., 2006).

3 Spatial resolution of OMI super-zoom mode

On-ground calibration measurements determined the footprint of an individual pixel to be near-Gaussian, spanning 2.3 detector row elements at nadir (~7 km FWHM) (Dobber et al., 2006). To determine an in-flight value, we compare the decay of MODIS (Fig. 1a) and OMI (Fig. 1b) broadband (459–479 nm) top-of-atmosphere reflectance over the Qatari coastline on 19 November 2004. MODIS reflectance is reported at a resolution of $500 \times 500\,m^2$. By comparing the MODIS and OMI observed reflectance across a sharp transition, such as a coastline, we can deduce a value for the spatial resolution of OMI. For a single transect (Fig. 1b and c), MODIS (red) observes a decrease in normalized reflectance from 0.8 to 0.2 over 3 km, a decrease that OMI (blue) observes over 9 km. Additionally, the width of an observed enhancement in NO_2

AMTD
4, 1989–2005, 2011

directly over and downwind of an isolated NO_x source is no wider than 6–9 km FWHM (PP4, Fig. 2b). Both of these in-flight tests provide an upper bound on instrumental spatial resolution (~9 km) that is in good agreement with on-ground calibration (7 km FWHM) (Dobber et al., 2006).

4 Slant column NO_2 from OMI super-zoom mode

From 1 October 2004 to 31 December 2004, OMI made 85 super-zoom orbits, 42 of those reporting observations at nadir. From these super-zoom observations, we retrieve slant column NO_2 from individual detector elements (i.e. super-zoom mode) and the average of eight detector elements (i.e. operational-scale) over the Rihand Reservoir in India (Fig. 2a–d; 23 November 2004; 82.5–83.5° E and 23.6–24.5° N), Seoul, South Korea (Fig. 2e–h; 21 November 2004; 126.7–127.7° E, 37.05–37.95° N), and Sarni, Madhya Pradesh, India (Fig. 2i–l; 19 November 2004; 77.7–78.7° E, 21.5–22.5° N). We have chosen these regions to highlight the super-zoom observations over a set of large point sources (Rihand), a megacity (Seoul), and a small point source (Sarni). We compare the single-overpass super-zoom observations to the average of six operational-scale overpasses from successive years between October and December on days when the selected region was cloud-free and nadir to the spacecraft (Rihand; 1 November 2005, 10 November 2005, 17 November 2005, 19 November 2005, 26 November 2005, 5 December 2005; Seoul; 23 October 2005, 8 November 2005, 12 October 2006, 11 November 2006, 20 November 2006, 7 November 2007; and Sarni; 30 October 2005, 6 November 2005, 22 November 2005, 8 December 2005, 18 November 2006, 11 December 2006). We use MODIS reflectance observations, taken aboard the Aqua platform, to serve as independent visual confirmation that the selected scenes are cloud-free (Fig. 2a, e, i).

Over the Rihand Reservoir (Fig. 2a–d), the super-zoom mode distinguishes three maxima in slant column NO_2 directly over or slightly downwind of three large coal-fired power plants (Fig. 2a–b; PP1 – 7.9×10^{16} molecules cm^{-2},

AMTD
4, 1989–2005, 2011

PP2 – 6.0×10^{16} molecules cm^{-2}, PP4 – 2.5×10^{16} molecules cm^{-2}) with the observed signal decreasing from maximum to near-background levels ($SCD_{NO_2} \approx 1.0 \times 10^{16}$ molecules cm^{-2}) within as little as 12 km, variability not detectable with the 13×24 km^2 operational footprint, which only observes one local maximum (Fig. 2c; 5.8×10^{16} molecules cm^{-2}). While spatial detail is increased by averaging six non-overlapping, operational-scale observations (Fig. 2d), the spatial contrast observed in the six-orbit average (Fig. 2d; $1\sigma - 0.6 \times 10^{16}$ molecules cm^{-2}) is a factor of 2.3 less than that observed by the super-zoom mode (Fig. 2b; $1\sigma - 1.4 \times 10^{16}$ molecules cm^{-2}). Furthermore, the six-orbit average is only able to distinguish one maximum (Fig. 2d; 3.7×10^{16} molecules cm^{-2}), a maximum that is 2.5 times smaller, if we assume a background of 1×10^{16} molecules cm^{-2} than that observed on a single day (Fig. 2b; 7.9×10^{16} molecules cm^{-2}).

Over Korea, a maximum in slant column NO_2 (Fig. 2f; 6.3×10^{16} molecules cm^{-2}) is observed ~12 km to the east of downtown Seoul with the signal decreasing from the maximum to near-background over a distance of 30–50 km. Because the decrease of signal occurs over a distance comparable to an operational-scale pixel (13×24 km^2), the operational-scale retrieval is able to capture the general structure of the Seoul urban-plume despite averaging out fine-scale details (Fig. 2g). The six-orbit operational-scale average (Fig. 2h) is much smoother than that observed in a single day (Fig. 2f–g), an effect of varying daily meteorology that is removed in the average.

Super-zoom observations capture a maximum in slant column NO_2 directly to the south of the Satpura Power Plant in Sarni, India (Fig. 2j; 2.2×10^{16} molecules cm^{-2}). When the signal in the super-zoom mode drops below $\sim 1.5 \times 10^{16}$ molecules cm^{-2} however, the variability is non-physical and noisy. At operational-scale, both single- and six-orbit average, the enhancement is modest relative to the background (Fig. 2k–l; 1.2 vs. 1.0×10^{16} molecules cm^{-2}). These observations indicate that the super-zoom mode accurately identifies the location of relatively small sources.

AMTD
4, 1989–2005, 2011

5 Uncertainty in slant column NO_2

In Fig. 3, we show the ratio of retrieved slant column NO_2 to the fitting error observed over Rihand, India, Seoul, South Korea, and Sarni, India, by both the super-zoom and operational modes of OMI. The fitting error ranges from 2.5 to 4×10^{15} molecules cm^{-2} for all super-zoom scenes and from 1.5 to 2.5×10^{15} molecules cm^{-2} for the analogous operational-scale observations (not shown). This decrease is smaller than $\sqrt{8}$ ($N_{operational} = 8 \times N_{super-zoom}$). Previous work shows that the fitting error is roughly equally determined by raw instrumental noise and the uncertainty in treatment of the temperature dependence of NO_2 absorption (Boersma et al., 2002). The fitting error retrieved for the super-zoom mode ($2.5 - 4 \times 10^{15}$ molecules cm^{-2}), is much lower than the detection threshold deduced previously (Sect. 4, Fig. 2j; 15×10^{15} molecules cm^{-2}), indicating that observations with SNR less than ~5–6 are unreliable. For all enhancements observed by the super-zoom mode, the SNR (Fig. 3a–d) is greater than 5 and as high as 25, evidence that fitting error and instrumental noise are not the limiting factors in producing high spatial-resolution maps of atmospheric NO_2 over large sources and multi-orbit averages of smaller sources.

6 Case study over Dubai, UAE

We compare slant column NO_2 retrieved from the 21 November 2004, super-zoom overpass of Dubai (55.0–55.7° E, 24.9–25.5° N), the corresponding operational-scale overpass, and that retrieved from six cloud-free operational-scale overpasses in late 2005 (Fig. 4; 23 October 2005, 30 October 2005, 1 November 2005, 8 November 2005, 1 December 2005, and 3 December 2005). We choose Dubai because the data set is relatively simple to interpret. Dubai is an isolated source of NO_x advected over a highly reflective, relatively homogenous desert surface. Over Dubai, we apply a destriping algorithm to the super-zoom observations by assuming that all high-frequency cross-track variability observed on the same orbit over the remote southwestern Indian

AMTD
4, 1989–2005, 2011

Ocean is unphysical, and subtract it from each along-track row; this approach is similar to those applied in previous studies (Boersma et al., 2007).

The spatial extent of the observed NO_2 enhancement is approximately 75 km SW–NE by 40 km SE–NW (Fig. 4c), about two times the size of the Dubai metropolitan area (Fig. 4b). Within the observed plume, slant column NO_2 is highly variable, with differences as much as 2×10^{16} molecules cm^{-2}(~50%) over 4 cross-track pixels (~12 km) or one row (13 km). The relative variability is even greater if the stratospheric contribution, which can be considered constant across the area of interest, is taken into account (~6×10^{15} molecules cm^{-2}). Adding confidence to the super-zoom observations, the area-weighted operational-scale retrieval (Fig. 4d) captures the same shape and detail of the plume ($75 \times 40\,km^2$), but is not able to capture the strong gradients observed by the super-zoom mode, the result of a coarser footprint and meteorological variability in the six-day average.

Due to the alignment of the OMI super-zoom footprint, variability of emissions along the Dubai coastline should be detectable (Fig. 4b and c). For example, the super-zoom mode observes an enhancement of slant column NO_2 directly over and downwind from the Jebel Ali Free Trade Zone (JAFTZ), a port and power generation center (A B, Fig. 4b and c). The enhancement directly over JAFTZ (A) is not as large as the enhancement downwind (B) because the source is near the leeward edge of the 13 km OMI pixel, which dilutes the signal with that of the clean marine background. Also, the time required to form NO_2 from reaction of NO and ozone is non-negligible for large point sources. The six-day area-weighted average (Fig. 4d) is not able to distinguish JAFTZ from the dense urban core to the northeast.

The decay of signal further downwind of JAFTZ (white box, Fig. 4b and c) can be used to assess the chemical lifetime of NO_2. Here, the plume evolves over a region of relatively little anthropogenic activity and the signal decreases from 2.45 to 1.55×10^{16} molecules cm^2 in the cross-track average (Fig. 2c, white box B to C). Given a stratospheric contribution to the slant column of 0.6×10^{16} molecules cm^{-2} and winds of $3\,m\,s^{-1}$ that project on the direction of observed decay by 0.8 (2–4 $m\,s^{-1}$)

AMTD
4, 1989–2005, 2011

winds observed at Dubai and Sharjah International Airports in the North, NOAA NCDC DS3505), this decrease in signal corresponds to an NO_2 lifetime of 1.9 h. At 30 °C (i.e., $k_{OH + NO_2} = 1.0 \times 10^{-11}$ molecules^{-1} cm^3 s^1), an NO_2 lifetime of 1.9 h corresponds to an OH concentration of 1.5×10^7 molecules cm^{-3}. This value is not unreasonable as noontime OH of 1.5–2.0 × 10^7 molecules cm^{-3} has been observed in late August and early September over Houston and La Porte, Texas, polluted marine environments at comparable latitude to Dubai. Furthermore, any uncertainty in wind speed (±1 m s^{-1}) corresponds to large uncertainty in implied OH (2 m s^{-1} – 1×10^7 molecules cm^{-3}, 4 m s^{-1} – 2×10^7 molecules cm^{-3}). Also under these conditions (Cleary et al., 2007), peroxyactetyl nitrate (PAN) formation is likely, reducing the apparent NO_2 lifetime and increasing the effective OH concentration derived from NO_2 decay. NO_2 stored as PAN is re-released downwind. The uncertainty in winds and chemistry are much larger than any variability of surface reflectance over the selected region (Fig. 4c, white box; 459–479 nm, OMI −0.22 ± 0.01; MODIS −0.17 ± 0.02), a potential interference for slant column variability.

These examples demonstrate a few advantages of utilizing measurements at higher spatial resolution than the current OMI (13 × 24 km^2) or GOME-2 (40 × 80 km^2) products. Future opportunities to provide this substantial advance in scientific capability include the proposed TROPOMI (Langen, 2007) and GEOCAPE (NRC, 2007) instruments. Such observations will enable the tracking of individual source regions within cities and allow for better assessment of chemistry in urban outflow.

7 Conclusions

We show that slant column NO_2 retrieved from the super-zoom mode of OMI has high signal to noise, has a similar spatial extent to that of single day and average operational-scale retrievals, and captures spatial variability at much finer scales than the 13 × 24 km^2 operational footprint. We take advantage of enhanced resolution reported in the super-zoom mode to distinguish large point sources in close

AMTD
4, 1989–2005, 2011

proximity around the Rihand Reservoir and distinguish the Jebel Ali Free Trade Zone, a Dubai port, from the Dubai urban center ~30 km to the northeast. We also derive an NO_2 chemical lifetime of 1.9 h and an effective OH concentration of 1.5×10^7 molecules cm^{-2} for a plume observed downwind of the Jebel Ali Free Trade Zone.

Acknowledgements. This work was supported by NASA under Grant #NNX08AE566, and by NASA Headquarters under the NASA Earth and Space Science Fellowship Program – Grant NESSF09, and CARB under Grant #06-328. We acknowledge the free use of Level 1 data from Aura-OMI from http://disc.sci.gsfc.nasa.gov/Aura/data-holdings/OMI. We thank NOAA-NCDC for providing non-commercial access to hourly observations of wind and temperature over Dubai, UAE, at http://cdo.ncdc.noaa.gov/. We appreciate the image provided by the Image Science and Analysis Laboratory, NASA Johnson Space Center, http://eol.jsc.nasa.gov/.

References

Boersma, K. F., Bucsela, E. J., Brinksma, E. J., and Gleason, J. F.: OMI Algorithm Theoretical Basis Document, OMI Trace Gas Algorithms, ATBD-OMI-04 (version 2), 2002.

Boersma, K. F., Eskes, H. J., Veefkind, J. P., Brinksma, E. J., van der A, R. J., Sneep, M., van den Oord, G. H. J., Levelt, P. F., Stammes, P., Gleason, J. F., and Bucsela, E. J.: Near-real time retrieval of tropospheric NO_2 from OMI, Atmos. Chem. Phys., 7, 2103–2118, doi:10.5194/acp-7-2103-2007, 2007.

Bogumil, K., Orphal, J., Burrows, J. P., and Flaud, J. M.: Vibrational progressions in the visible and near-ultraviolet absorption spectrum of ozone, Chem. Phys. Lett., 349, 241–248, 2001.

Bucsela, E. J., Celarier, E. A., Wenig, M. O., Gleason, J. F., Veefkind, J. P., Boersma, K. F., and Brinksma, E. J.: Algorithm for NO_2 vertical column retrieval from the Ozone Monitoring Instrument, IEEE T. Geosci. Remote, 44, 1245–1258, doi:10.1109/TGRS.2005.863715, 2006.

Celarier, E. A., Brinksma, E. J., Gleason, J. F., Veefkind, J. P., Cede, A., Herman, J. R., Ionov, D., Goutail, F., Pommereau, J. P., Lambert, J. C., van Roozendael, M., Pinardi, G., Wittrock, F., Schonhardt, A., Richter, A., Ibrahim, O. W., Wagner, T., Bojkov, B., Mount, G., Spinei, E.,

AMTD
4, 1989–2005, 2011

Chen, C. M., Pongetti, T. J., Sander, S. P., Bucsela, E. J., Wenig, M. O., Swart, D. P. J., Volten, H., Kroon, M., and Levelt, P. F.: Validation of Ozone Monitoring Instrument nitrogen dioxide columns, J. Geophys. Res.-Atmos., 113, D15S15, doi:10.1029/2007JD008908, 2008.

Chance, K. V. and Spurr, R. J. D.: Ring effect studies: Rayleigh scattering, including molecular parameters for rotational Raman scattering, and the Fraunhofer spectrum, Appl. Optics, 36, 5224–5230, 1997.

Cleary, P. A., Wooldridge, P. J., Millet, D. B., McKay, M., Goldstein, A. H., and Cohen, R. C.: Observations of total peroxy nitrates and aldehydes: measurement interpretation and inference of OH radical concentrations, Atmos. Chem. Phys., 7, 1947–1960, doi:10.5194/acp-7-1947-2007, 2007.

Dobber, M. R., Dirksen, R. J., Levelt, P. F., Van den Oord, G. H. J., Voors, R. H. M., Kleipool, Q., Jaross, G., Kowalewski, M., Hilsenrath, E., Leppelmeier, G. W., de Vries, J., Dierssen, W., and Rozemeijer, N. C.: Ozone Monitoring Instrument calibration, IEEE T. Geosci. Remote, 44, 1209–1238, doi:10.1109/tgrs.2006.869987, 2006.

Dobber, M. R., Kleipool, Q., Dirksen, R., Levelt, P., Jaross, G., Taylor, S., Kelly, T., Flynn, L., Leppelmeier, G., and Rozemeijer, N.: Validation of Ozone Monitoring Instrument level 1b data products, J. Geophys. Res.-Atmos., 113, D15S06, doi:10.1029/2007JD008665, 2008.

Earth science and applications from space: National imperatives for the next decade and beyond, National Research Council of the National Academies, The National Academies Press, Washington, DC, 2007.

Jaegle, L., Steinberger, L., Martin, R. V., and Chance, K.: Global partitioning of NO_x sources using satellite observations: Relative roles of fossil fuel combustion, biomass burning and soil emissions, Faraday Discuss., 130, 407–423, 2005.

Kim, S. W., Heckel, A., McKeen, S. A., Frost, G. J., Hsie, E. Y., Trainer, M. K., Richter, A., Burrows, J. P., Peckham, S. E., and Grell, G. A.: Satellite-observed US power plant NO_x emission reductions and their impact on air quality, Geophys. Res. Lett., 33(5), L22812, doi:10.1029/2006gl027749, 2006.

Konovalov, I. B., Beekmann, M., Richter, A., and Burrows, J. P.: Inverse modelling of the spatial distribution of NO_x emissions on a continental scale using satellite data, Atmos. Chem. Phys., 6, 1747–1770, doi:10.5194/acp-6-1747-2006, 2006

Langen, J.: GMES Sentinels 4 and 5 mission requirements document, European Space Agency, 2007.

Levelt, P. F., Hilsenrath, E., Leppelmeier, G. W., van den Oord, G. H. J., Bhartia, P. K., Tammi-

nen, J., de Haan, J. F., and Veefkind, J. P.: Science objectives of the Ozone Monitoring Instrument, IEEE T. Geosci. Remote, 44, 1199–1208, doi:10.1109/tgrs.2006.872336, 2006a.
Levelt, P. F., Van den Oord, G. H. J., Dobber, M. R., Malkki, A., Visser, H., de Vries, J., Stammes, P., Lundell, J. O. V., and Saari, H.: The Ozone Monitoring Instrument, IEEE T. Geosci. Remote, 44, 1093–1101, doi:10.1109/tgrs.2006.872333, 2006b.
Loughner, C. P., Lary, D. J., Sparling, L. C., Cohen, R. C., DeCola, P., and Stockwell, W. R.: A method to determine the spatial resolution required to observe air quality from space, IEEE T. Geosci. Remote, 45, 1308–1314, doi:10.1109/tgrs.2007.893732, 2007.
Martin, R. V., Jacob, D. J., Chance, K., Kurosu, T. P., Palmer, P. I., and Evans, M. J.: Global inventory of nitrogen oxide emissions constrained by space-based observations of NO_2 columns, J. Geophys. Res.-Atmos., 108, 4537, doi:10.1029/2003JD003453, 2003.
Platt, U. and Stutz, J.: Differential optical absorption spectroscopy principles and applications, Physics of Earth and Space Environments, Springer Verlag, Berlin, 15, 597 pp., 2008.
Richter, A., Burrows, J. P., Nuss, H., Granier, C., and Niemeier, U.: Increase in tropospheric nitrogen dioxide over China observed from space, Nature, 437, 129–132, doi:10.1038/nature04092, 2005.
Russell, A. R., Valin, L. C., Bucsela, E. J., Wenig, M. O., and Cohen, R. C.: Space-based constraints on spatial and temporal patterns of NO_x emissions in California, 2005–2008, Environ. Sci. Technol., 44, 3608–3615, doi:10.1021/es903451j, 2010.
Schoeberl, M. R., Douglass, A. R., Hilsenrath, E., Bhartia, P. K., Beer, R., Waters, J. W., Gunson, M. R., Froidevaux, L., Gille, J. C., Barnett, J. J., Levelt, P. E., and DeCola, P.: Overview of the EOS-AURA mission, IEEE T. Geosci. Remote, 44, 1066–1074, doi:10.1109/tgrs.2005.861950, 2006.
Toenges-Schuller, N., Stein, O., Rohrer, F., Wahner, A., Richter, A., Burrows, J. P., Beirle, S., Wagner, T., Platt, U., and Elvidge, C. D.: Global distribution pattern of anthropogenic nitrogen oxide emissions: Correlation analysis of satellite measurements and model calculations, J. Geophys. Res.-Atmos., 111, D05312, doi:10.1029/2005JD006068, 2006.
Van den Oord, G. H. J., Rozemeijer, N. C., Schenkelaars, V., Levelt, P. F., Dobber, M. R., Voors, R. H. M., Claas, J., De Vries, J., Ter Linden, M., De Haan, C., and de Berg, T. V.: OMI level 0 to 1b processing and operational aspects, IEEE T. Geosci. Remote, 44, 1380–1397, doi:10.1109/tgrs.2006.872935, 2006.
Vandaele, A. C., Hermans, C., Fally, S., Carleer, M., Colin, R., Merienne, M. F., Jenouvrier, A., and Coquart, B.: High-resolution Fourier transform measurement of the NO_2 visible

AMTD
4, 1989–2005, 2011

Observation of slant column NO_2 using the super-zoom mode of AURA-OMI

L. C. Valin et al.

and near-infrared absorption cross sections: Temperature and pressure effects, J. Geophys. Res.-Atmos., 107, 4348, doi:10.1029/2001jd000971, 2002.
Wenig, M., Jahne, B. J., and Platt, U.: Operator representation as a new differential optical absorption spectroscopy formalism, Appl. Optics, 44, 3246–3253, 2005.

AMTD
4, 1989–2005, 2011

Observation of slant column NO_2 using the super-zoom mode of AURA-OMI

L. C. Valin et al.

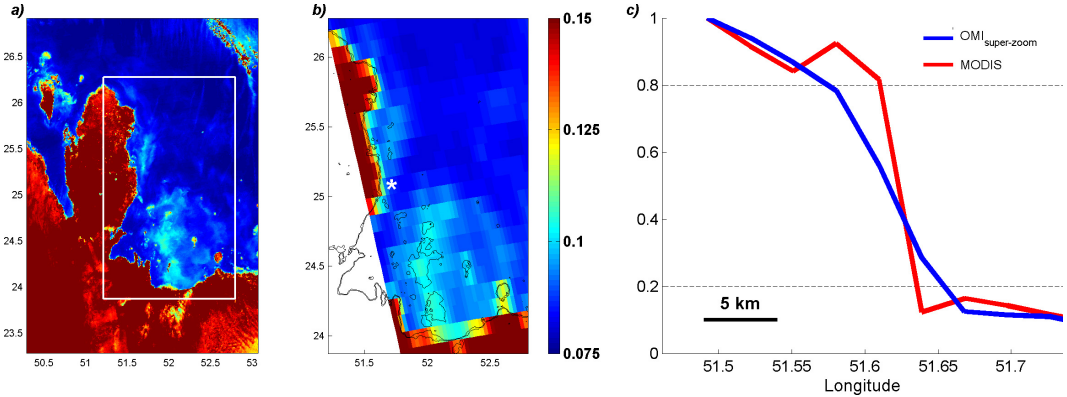

Fig. 1. Top-of-atmosphere reflectance (459–479 nm) observed by **(a)** MODIS and **(b)** the super-zoom mode of OMI over Qatar on 19 November 2004. **(c)** Top-of-atmosphere reflectance observations (MODIS – blue, OMI – red) are normalized along a transect perpendicular to the Qatari coastline **(b)**.

AMTD
4, 1989–2005, 2011

Observation of slant column NO_2 using the super-zoom mode of AURA-OMI

L. C. Valin et al.

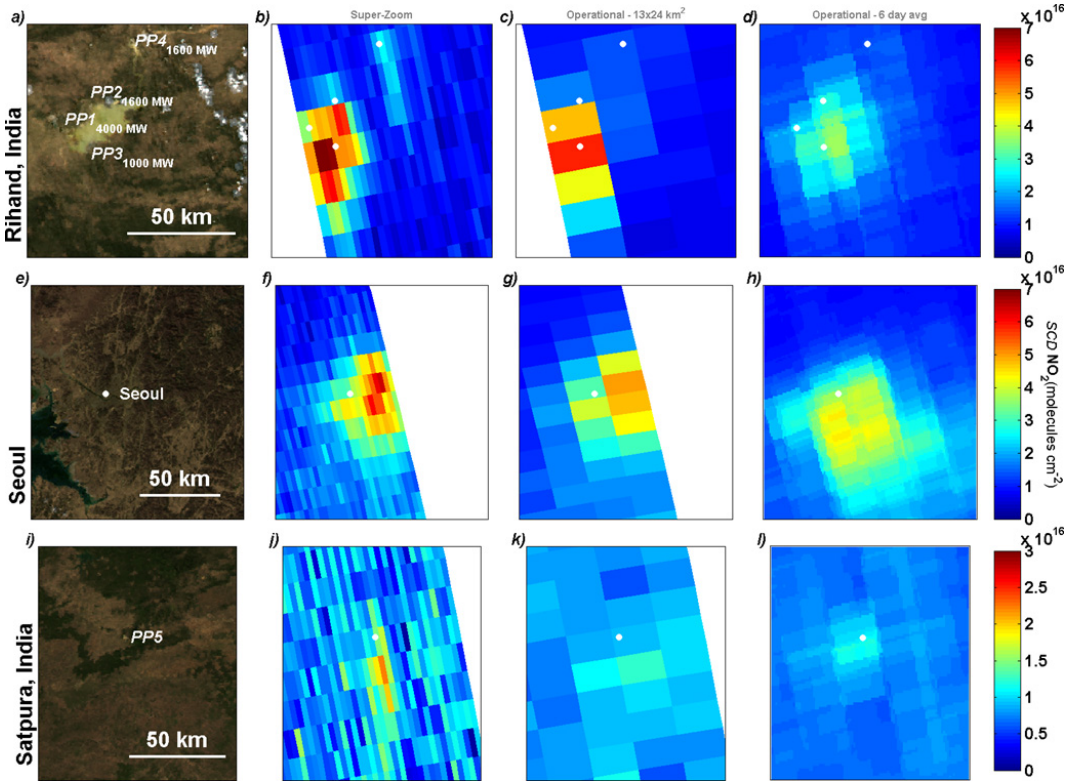

Fig. 2. MODIS RGB image, OMI super-zoom mode slant column NO_2 (SCD_{NO_2}), operational mode SCD_{NO_2}, and a six-orbit operational average SCD_{NO_2} over the Rihand Resovoir in India **(a–d)**, Seoul, South Korea **(e–h)**, and Sarni, India **(i–l)**. Power plants located around the Rihand Reservoir include Singrauli and Vindhyachal (PP1 – 4200 MW), Anpara (PP2 – 1600 MW), Rihand (PP3 – 1000 MW pre-2006), and Obra (PP4 – 1600 MW). Power plants around Sarni, India **(i)**, include Satpura generating station (PP5).

AMTD
4, 1989–2005, 2011

Observation of slant column NO_2 using the super-zoom mode of AURA-OMI

L. C. Valin et al.

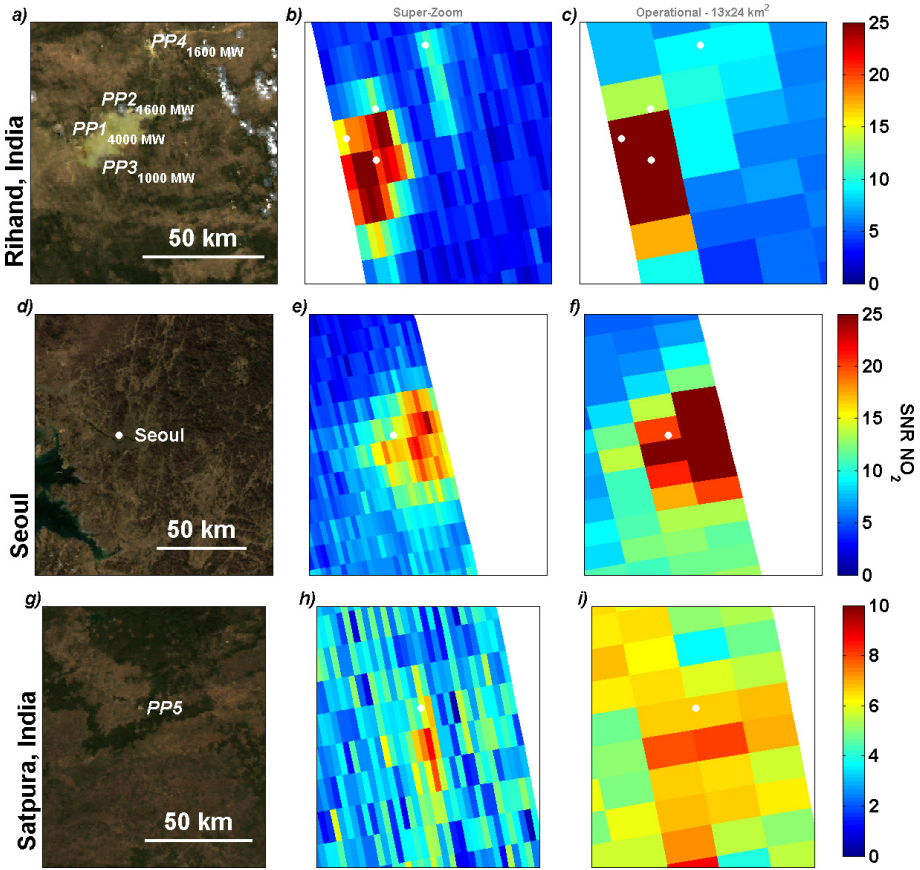

Fig. 3. MODIS RGB image and ratio of slant column NO_2 to NO_2 fit precision (SNR) for super-zoom and operational retrievals over the Rihand Resovoir in India **(a–c)**, Seoul, South Korea **(d–f)**, and Sarni, India **(g–i)**, respectively. For information on the power plants labeled (PP1–5), see Fig. 2.

AMTD
4, 1989–2005, 2011

Observation of slant column NO_2 using the super-zoom mode of AURA-OMI

L. C. Valin et al.

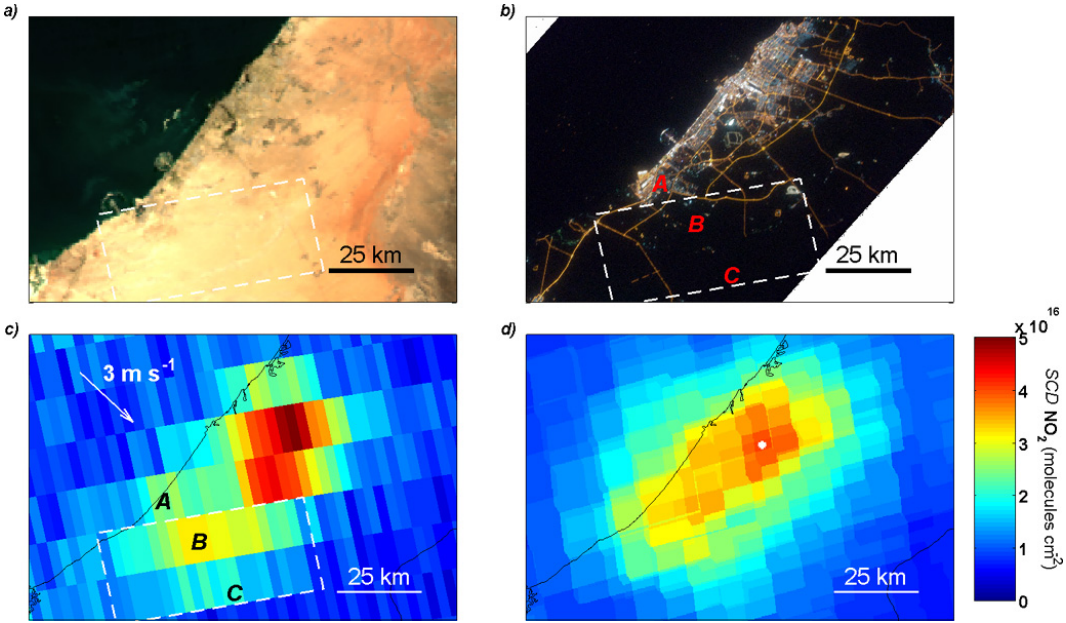

Fig. 4. **(a)** True color image from Aqua-MODIS on 21 November 2004. **(b)** Nighttime image (courtesy of the Image Science and Analysis Laboratory, NASA Johnson Space Center, ISS020-E-39932) captured aboard the International Space Station over Dubai, UAE, on 11 September 2009 at 02:00 LST. **(c)** Slant column NO_2 retrieved from a single overpass on 08:42 GMT, 21 November 2004 for individual pixels and **(d)** a six-orbit, area-weighted average of slant column NO_2 retrieved from operational mode orbits during October, November and December of 2005 Labels A, B and C in **(b–c)** highlight the locations of the Jebel Ali Free Zone and points on a downwind transect. The white arrow in **(c)** indicates the direction and magnitude of winds observed at the Sharjah and Dubai International Airports around midday on 21 November 2004 (NOAA NCDC DS3505).

AMTD
4, 1989–2005, 2011

Observation of slant column NO_2 using the super-zoom mode of AURA-OMI

L. C. Valin et al.